You might find this additional information useful...

This article cites 51 articles, 15 of which you can access free at:
http://ajpheart.physiology.org/cgi/content/full/294/3/H1197#BIBL

Updated information and services including high-resolution figures, can be found at:
http://ajpheart.physiology.org/cgi/content/full/294/3/H1197

Additional material and information about *AJP - Heart and Circulatory Physiology* can be found at:
http://www.the-aps.org/publications/ajpheart

This information is current as of March 17, 2008 .

Heterogeneous transmural proteoglycan distribution provides a mechanism for regulating residual stresses in the aorta

Evren U. Azeloglu, Michael B. Albro, Vikrum A. Thimmappa, Gerard A. Ateshian, and Kevin D. Costa

Department of Biomedical Engineering, Columbia University, New York, New York

Azeloglu EU, Albro MB, Thimmappa VA, Ateshian GA, Costa KD. Heterogeneous transmural proteoglycan distribution provides a mechanism for regulating residual stresses in the aorta. *Am J Physiol Heart Circ Physiol* 294: H1197–H1205, 2008. First published December 21, 2007; doi:10.1152/ajpheart.01027.2007.—The arterial wall contains a significant amount of charged proteoglycans, which are inhomogeneously distributed, with the greatest concentrations in the intimal and medial layers. The hypothesis of this study is that the transmural distribution of proteoglycans plays a significant role in regulating residual stresses in the arterial wall. This hypothesis was first tested theoretically, using the framework of mixture theory for charged hydrated tissues, and then verified experimentally by measuring the opening angle of rat aorta in NaCl solutions of various ionic strengths. A three-dimensional finite element model of aortic ring, using realistic values of the solid matrix shear modulus and proteoglycan fixed-charge density, yielded opening angles and changes with osmolarity comparable to values reported in the literature. Experimentally, the mean opening angle in isotonic saline (300 mosM) was 15 ± 17° and changed to 4 ± 19° and 73 ± 18° under hypertonic (2,000 mosM) and hypotonic (0 mosM) conditions, respectively (*n* = 16). In addition, the opening angle in isotonic (300 mosM) sucrose, an uncharged molecule, was 60 ± 16° (*n* = 11), suggesting that the charge effect, not cellular swelling, was the major underlying mechanism for these observations. The extent of changes in opening angle under osmotic challenges suggests that transmural heterogeneity of fixed-charge density plays a crucial role in governing the zero-stress configuration of the aorta. A significant implication of this finding is that arterial wall remodeling in response to altered wall stresses may occur via altered deposition of proteoglycans across the wall thickness, providing a novel mechanism for regulating mechanical homeostasis in vascular tissue.

zero stress; glycosaminoglycans; vascular mechanics

IT HAS BECOME WIDELY RECOGNIZED that vascular tissue supports a self-equilibrating internal residual stress in the unloaded intact state (16). The presence of significant residual stress is most notably demonstrated by the tendency of rings of the arterial wall to open when cut radially (8, 49). From a biomechanical standpoint, residual stresses (and the associated residual strains) play a key role in the identification of an appropriate "zero-stress" reference configuration and hence impact the definition of mechanical stresses and strains in the tissue (8, 23, 34). From a physiological standpoint, knowledge of the mechanisms underlying acute and chronic changes in residual stress are also required for understanding how growth and remodeling influence the mechanical homeostasis in vascular tissue (22, 30, 32, 46, 47).

Although the functional importance of cardiovascular residual stresses is reasonably well accepted (22, 38), identifying the specific mechanisms underlying their existence remains an area of active investigation. One theory suggests that residual stresses result from elastic deformations required to ensure kinematic compatibility in the presence of local tissue growth (41). Others have shown that residual stress is strongly dependent on heterogeneity of material properties across the vessel wall (48). Although the dissolving of collagen has no effect on opening angle (17), elastin appears to be partially responsible for residual stresses in arteries (43), although more recent reports have challenged this finding (54). Rapid changes in opening angle have been shown to occur as a result of changes in bathing solution osmolarity, purportedly due to swelling of the cellular component of the left ventricular (29) or aortic (20) vessel wall. However, in another study, destroying smooth muscle cells by freezing had no effect on arterial opening angle (17). Regional variations of opening angle (31) and elastic modulus (19) with anatomic location have also been reported. In summary, no explicit mechanism has been described to date that can explain how these residual stresses might be induced and why they might vary along the length of arteries such as the aorta.

In contrast, in the field of cartilage mechanics, it has long been known that residual stresses arise from the Donnan osmotic pressure, which results from the presence of negatively charged proteoglycans enmeshed within the collagen matrix (28, 33), and curling behavior similar to that shown in arterial wall segments has been observed, consistent with the evolution of residual stresses due to changes in the tissue's ionic environment (45).

Indeed, the arterial wall contains a substantial amount of proteoglycans (56, 57), which are inhomogeneously distributed across the wall, showing a greater concentration in the intimal and medial layers than in the adventitia. From these observations, we hypothesize that the transmural distribution of proteoglycans plays a significant role in regulating the residual stresses in the arterial wall. This hypothesis is first tested theoretically, to determine whether realistic values of material properties of the arterial wall and charge density of the proteoglycans can predict opening angles in the range observed in the prior literature. It is then tested experimentally by performing osmotic loading experiments on the excised rat aorta and measuring changes in the opening angle. A counterhypothesis, that the opening angle may be regulated by osmotic swelling of vascular smooth muscle cells, rather than Donnan swelling resulting from the extracellular proteoglycans, is also tested by

replacing charged membrane-impermeant osmolytes with uncharged ones; from experimental findings, this is found to play only a minor role.

THEORETICAL ANALYSIS

The theoretical framework for analyzing residual stresses resulting from negatively charged proteoglycans in a tissue bathing in a binary electrolyte solution of monovalent salt ions is the triphasic theory of Lai et al. (28). For simplicity, only the equilibrium response to changes in the ionic environment is considered here. The basic premise of the theory is that the total Cauchy stress

$$\mathbf{T} = -p\mathbf{I} + \mathbf{T}^e \qquad (1)$$

is the sum of the hydrostatic fluid pressure (p) and the effective (or elastic) stress in the solid matrix ($\mathbf{T}^e$); $\mathbf{I}$ is the identity tensor. Under equilibrium conditions, when the solid and fluid velocities have reduced to zero, p reduces to the Donnan osmotic pressure (36),

$$p - p^* = R\theta\left[\sqrt{(c^F)^2 + (\bar{c}^*)^2} - \bar{c}^*\right] \qquad (2)$$

where p^* is the ambient pressure in the external bath (henceforth taken to be zero, $p^* = 0$), c^F is the proteoglycan fixed-charge density, $\bar{c}^*$ is the external bath salt osmolarity ($\bar{c}^* = 2c^*$, where c^* is the salt concentration), R is the universal gas constant, and θ is absolute temperature. This relation assumes that the interstitial fluid and external bath solutions (water solvent and electrolytes) are ideal, although it can be easily formulated for real solutions with the introduction of nonunity activity and osmotic coefficients (1, 28, 36). From the equation of conservation of mass for the solid matrix, c^F is kinematically related to the solid matrix relative volume change ($J = \det\mathbf{F}$) via

$$c^F = \varphi_0^w c_0^F / (J - 1 + \varphi_0^w) \qquad (3)$$

where $\mathbf{F}$ is the deformation gradient of the solid matrix, and c_0^F and ϕ_0^w are the fixed-charge density and water content in the strain-free reference configuration. For a hyperelastic solid matrix, the general form of the elastic stress is

$$\mathbf{T}^e = 2J^{-1}\mathbf{F}\frac{\partial W}{\partial \mathbf{C}}\mathbf{F}^T \qquad (4)$$

where $\mathbf{C} = \mathbf{F}^T\mathbf{F}$ is the right Cauchy-Green deformation tensor and $W(\mathbf{C})$ is a strain energy density function dependent on the particular choice of constitutive relation for the solid.

The governing equation to solve for the equilibrium swelling response is the conservation of momentum for the mixture,

$$\mathrm{div}\mathbf{T} = -\mathrm{grad}\,p + \mathrm{div}\mathbf{T}^e = \mathbf{0} \qquad (5)$$

Because p is dependent on J according to *Eqs. 2* and *3* and $\mathbf{T}^e$ is a function of $\mathbf{C}$, *Eq. 5* can be solved for the unknown solid displacement ($\mathbf{u}$), given that $\mathbf{F} = \mathbf{I} + \mathrm{Grad}\mathbf{u}$, on the suitable application of displacement and traction boundary conditions, $\mathbf{u}^*$ and $\mathbf{t}^* = \mathbf{T}\mathbf{n}$, respectively, where $\mathbf{n}$ is the outward normal to the surface.

An examination of these equations shows that the strain-free reference configuration can be achieved under traction-free boundary conditions when the external bath is strongly hyper-

tonic ($\bar{c}^* \rightarrow \infty$). Under this hypertonic state, the Donnan osmotic pressure difference between the tissue's interstitial fluid and the external bath reduces to zero according to *Eq. 2*, so that *Eq. 5* reduces to $\mathbf{T}^e = 0$. In the absence of residual stresses resulting from mechanisms other than osmotic swelling, this equation produces $\mathbf{T}^e = 0$ and $\mathbf{C} = \mathbf{I}$ under traction-free boundary conditions ($\mathbf{t}^* = 0$). That is, residual stress and opening angle (i.e., deformation) should approach zero in the limit as fixed-charge effects are neutralized by a very hypertonic bathing solution.

FINITE ELEMENT ANALYSIS

A custom three-dimensional finite element program was written to solve these equations under finite deformation. It is noteworthy that these equations are very similar to those of classical finite elasticity theory, which facilitates the finite element implementation considerably. Whereas the stress tensor in classical elasticity would be given only by $\mathbf{T}^e$ in *Eq. 4*, the swelling analysis requires the use of $\mathbf{T}$ in *Eq. 1*, where the dependence of p on J is given in *Eqs. 2* and *3*. Similarly, the spatial elasticity tensor is given by

$$\mathbf{C} = \mathbf{\Pi} + \mathbf{C}^e \qquad (6)$$

where

$$C^e = 4J^{-1}(\mathbf{F}\underline{\otimes}\mathbf{F}):\frac{\partial^2 W}{\partial\mathbf{C}^2}:(\mathbf{F}^T\underline{\otimes}\mathbf{F}^T) \qquad (7)$$

is the spatial elasticity tensor for the solid matrix and

$$\mathbf{\Pi} = J^{-1}(\mathbf{F}\underline{\otimes}\mathbf{F}):2\frac{\partial(-Jp\mathbf{C}^{-1})}{\partial\mathbf{C}}:(\mathbf{F}^T\underline{\otimes}\mathbf{F}^T) = -J\frac{\partial p}{\partial J}\mathbf{I}\otimes\mathbf{I} \\ + p(2\mathbf{I}\,\overline{\underline{\otimes}}\,\mathbf{I} - \mathbf{I}\otimes\mathbf{I}) \qquad (8)$$

is the tensor of the osmotic modulus, which results in part from the change in osmotic pressure with change in tissue volume (1, 4).[1] Note that this finite deformation formulation of the osmotic modulus is more general than the small-strain analysis reported in our earlier study (1).

For ideal solutions, the expression of *Eq. 2* can be combined with the general expression of *Eq. 3* to yield

$$\mathbf{\Pi} = \frac{R\theta J(c^F)^2}{(J - 1 + \varphi_0^w)\sqrt{(c^F)^2 + (\bar{c}^*)^2}}\mathbf{I}\otimes\mathbf{I} \\ + R\theta\left[\sqrt{(c^F)^2 + (\bar{c}^*)^2} - \bar{c}^*\right](2\mathbf{I}\,\overline{\underline{\otimes}}\,\mathbf{I} - \mathbf{I}\otimes\mathbf{I}) \qquad (9)$$

For consistency with experimental stress-strain data from mouse aorta at low lumen pressure (19), a neo-Hookean constitutive relation is selected for the solid matrix (2, 3),

$$\mathbf{T}^e = J^{-1}[\mu_s(\mathbf{B} - \mathbf{I}) + \lambda_s(\ln J)\mathbf{I}] \qquad (10)$$

$$C^e = J^{-1}[\lambda_s\mathbf{I}\otimes\mathbf{I} + 2(\mu_s - \lambda_s\ln J)\mathbf{I}\,\overline{\underline{\otimes}}\,\mathbf{I}] \qquad (11)$$

where $\mathbf{B} = \mathbf{F}\mathbf{F}^T$ is the left Cauchy-Green deformation tensor and λ_s and μ_s are Lamé-like material constants for the solid matrix. To explore whether the choice of constitutive relation significantly influences the outcome of the analysis, a Fung-

---

[1] See Ref. 10 for a definition of tensor dyadic products $\otimes$, $\underline{\otimes}$ and $\overline{\underline{\otimes}}$.

type exponential constitutive relation was also considered (11, 50), specialized to isotropic symmetry for simplicity,

$$\mathbf{T}^e = \frac{e^Q}{2J}\left[\lambda_s(\text{tr}\,\mathbf{B} - 3)\mathbf{B} + 2\mu_s(\mathbf{B}^2 - \mathbf{B})\right] \quad (12)$$

$$C^e = \frac{J}{ce^Q}\mathbf{T}^e \otimes \mathbf{T}^e + J^{-1}e^Q(\lambda_s\mathbf{B} \otimes \mathbf{B} + 2\mu_s\mathbf{B}\,\overline{\underline{\otimes}}\,\mathbf{B}) \quad (13)$$

where

$$Q = \frac{1}{4c}\left[\frac{\lambda_s}{2}(\text{tr}\,\mathbf{B} - 3)^2 + \mu_s(\text{tr}\,\mathbf{B}^2 - 2\text{tr}\,\mathbf{B} + 3)\right] \quad (14)$$

In this constitutive relation, λ_s and μ_s are similarly Lamé-like material constants and c is an additional elastic modulus (with units of force per area) that regulates the exponential rise.

In the special case when a tissue has homogeneous solid matrix properties and fixed-charge density and is subjected to traction-free boundary conditions (no displacement constraints), it is straightforward to show that the deformation gradient may be given by $\mathbf{F} = \lambda\mathbf{I}$, where λ is the stretch ratio representing the uniform, isotropic swelling of the tissue under various external bath osmolarities ($\bar{c}^*$). In the case of the neo-Hookean constitutive model, λ must satisfy

$$\mu_s(\lambda^2 - 1) + 3\lambda_s(\ln\lambda)$$
$$- \lambda^3 R\theta\left[\sqrt{\left(\frac{\varphi_0^w c_0^F}{\lambda^3 - 1 + \varphi_0^w}\right)^2 + (\bar{c}^*)^2} - \bar{c}^*\right] = 0 \quad (15)$$

In this special case, the opening angle of a cut aortic ring would be zero, since the resulting residual stresses would be homogeneous.

A three-dimensional finite element mesh of a ring of tissue from a rat aorta was created using average dimensions from the experimental results: 1.92 mm outer diameter, 0.137 mm wall thickness, and 1.09 mm slice thickness. From symmetry considerations, only one-quarter of the ring was modeled; 1,387 nodes and 240 20-node triquadratic brick elements were used in this finite element analysis. The wall thickness was divided equally into five layers of elements. The fixed-charge density in the strain-free reference configuration was prescribed at $c_0^F = 40$ meq/l in the intima and media (first and second layers through the wall thickness), 0 meq/l in the adventitia (fourth and fifth layers), and 20 meq/l in a transition zone (third layer); this magnitude of the fixed-charged density was based on measurements previously reported in the literature (37), whereas the distribution across the arterial wall thickness was based qualitatively on histological slides from this study (see below).

The water content in the reference configuration was uniformly set at $\phi_0^w = 0.7$ (22). For neo-Hookean and Fung constitutive models, a shear modulus $\mu_s = 140$ kPa was prescribed throughout the arterial wall (11), with $\lambda_s = 0$. This value of λ_s implies that the equilibrium Poisson ratio under free-draining and hypertonic loading conditions is zero; however, the tissue as a whole is incompressible under hydrostatic pressurization or in the short-term response to loading (2). In addition, for the Fung exponential model, a value of $c = 140$ kPa was selected to produce a modest rise in stiffness with increasing tensile stretch. The external bath concentration was varied from a hypertonic state ($\bar{c}^* = 4,000$ mosM) to a

hypotonic state ($\bar{c}^* = 2$ mosM) using 30 logarithmic increments. Because subsequent experiments were run at room temperature, the absolute temperature in the computational analysis was set to 298°K.

Variations in this baseline model were also examined, as described in RESULTS.

EXPERIMENTAL MATERIALS AND METHODS

All animals received humane care, and the procedures used were approved by the Columbia University Institutional Animal Care and Use Committee. The experimental study consisted of examining changes in the opening angle of radially cut aortic rings in response to alterations in the ionic strength or osmolarity of the external bath. Adult male Sprague-Dawley rats (Taconic Farms, Germantown, NY) were euthanized by CO_2 narcosis ($n = 2$) or anesthetized by isoflurane ($n = 2$), and the entire length of the thoracic aorta was isolated after midsternal thoracotomy. The vessel was allowed to equilibrate in cold PBS for 30 min and subsequently dissected into 8–10 rings ($n = 37$ rings total, from the 4 rats), which were randomly distributed among the different testing protocols described below to prevent bias with respect to anatomic location and placed into isotonic saline (300 mosM NaCl). This and all subsequent bathing solutions were supplemented with 4 μM cytochalasin D (Sigma, St. Louis, MO) to eliminate active cell contraction. Solution osmolarity was verified with a freezing point osmometer (model 3D3; Advanced Instruments, Norwood, MA). Each ring was radially cut and imaged under a dissecting microscope every 10 min throughout the experimental protocol described below. The opening angle was measured by an operator blinded to the osmotic condition, using the angle tool in the public domain image processing software ImageJ (http://rsb.info.nih.gov/ij).

After 60 min in isotonic saline, some of the samples ($n = 8$) were placed into hypotonic (0 mosM) solution for a 30-min osmotic challenge. Samples were then moved back to isotonic solution for another 30-min period, then transferred into a hypertonic (2,000 mosM NaCl) bath for 30 min, and finally returned to isotonic solution for 30 min. To test reversibility, the converse protocol was also performed with different samples ($n = 8$) equilibrated in isotonic solution (60 min) and then first osmotically challenged hypertonically (30 min), returned to isotonic conditions (30 min), then challenged hypotonically (30 min), and finally returned back to isotonic conditions (30 min).

The media and intima are highly cellularized tissues. It is well known that isolated cells change significantly in volume in response to osmotic loading with a plasma membrane-impermeant osmolyte (55). Thus a potential confounding factor is that changes in the opening angle observed in response to osmotic challenge with NaCl may be due to in situ cellular dilatation in the media and intima, rather than swelling of the charged extracellular matrix. To separate these effects, a second osmotic challenge protocol was devised using isotonic solution of charged NaCl and a solution of uncharged sucrose of equal osmolarity. Both NaCl and sucrose are membrane-impermeant osmolytes (over the time scale of the experiments conducted here), but only the electrolytic NaCl can influence the Donnan osmotic pressure in the charged extracellular matrix. Therefore, switching from isotonic saline to isotonic sucrose would produce no change in opening angle unless proteoglycans play an important role. A more detailed rationale for distinguishing the effects of cellular osmotic swelling from extracellular Donnan osmotic swelling is provided in DISCUSSION. In this second protocol, radially cut aortic ring samples ($n = 11$) were moved from 300 mosM NaCl to 300 mosM sucrose and back and then moved to 0 mosM NaCl and back to isotonic to compare the dilatory effects of sucrose and hypotonic solution.

To validate the fixed-charge density presumed in our finite-element model, mean glycosaminoglycan (GAG) content in the rat thoracic aorta was quantified using the 1,9-dimethylmethylene blue (DMMB) dye binding assay as previously described (15). Briefly, 2- to 3-cm

aortic samples from six additional Sprague-Dawley rats were isolated and padded dry for ~60 s until all external water was removed. Samples were then weighed on an ultrasensitive digital scale (M220-D; Denver Instrument, Denver, CO) for their wet weight and subsequently lyophilized for 72 h to obtain dry weight and total water content. After samples were weighed, the dried tissue was then digested with papain for 24 h and assayed for GAG content with DMMB using chondroitin-6-sulfate as the standard (15, 44).

Finally, a separate set of untested intact aortic rings from a similar anatomic location was fixed in 3.7% formaldehyde in PBS, dehydrated in steps, and embedded in glycol methacrylate resin (Tehnovit 7100; Kulzer, Wehrheim, Germany). Rings were sliced into 5-μm sections on a microtome and stained with hematoxylin and eosin for cell and tissue structure and with Safranin-O for GAG distribution.

All results are presented as means ± SD. We used the software SuperANOVA (Abacus Concepts, Berkeley, CA) for statistical analyses of opening angle results from each stage of the osmotic loading protocol for individual tissue samples, via multivariate repeated-measures ANOVA, so that each aortic ring effectively served as its own control. Single-factor ANOVA was used to examine the interaction effect of loading history for the two converse osmotic challenge protocols. Post hoc analysis was based on the least squares means, with Bonferroni correction for multiple pair-wise comparisons. Significance was accepted at the 95% confidence level.

RESULTS

Theoretical analysis. A rendering of the cut aortic ring geometry at selected external bath osmolarities is shown in Fig. 1 for the baseline model configuration, using the neo-Hookean constitutive relation for the solid matrix. Finite element results show that a ring, which is initially closed, has an opening angle of 5° at 2,000 mosM, 37° under isotonic conditions (300 mosM), and 206° under hypotonic conditions (2 mosM). A plot of the opening angle vs. $\bar{c}^*$ for all 30 increments of the finite element analysis is presented in Fig. 2; below $\bar{c}^* = 20$ mosM, the opening angle remains nearly constant; above $\bar{c}^* = 100$ mosM, the linear variation on a log-log scale, with a slope of
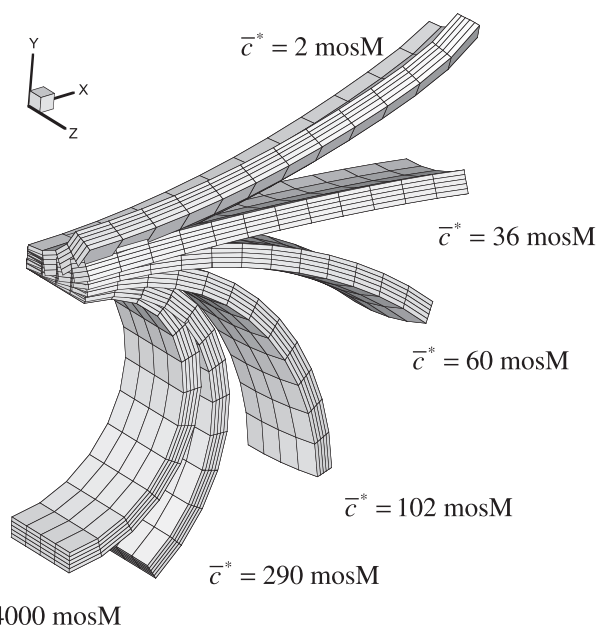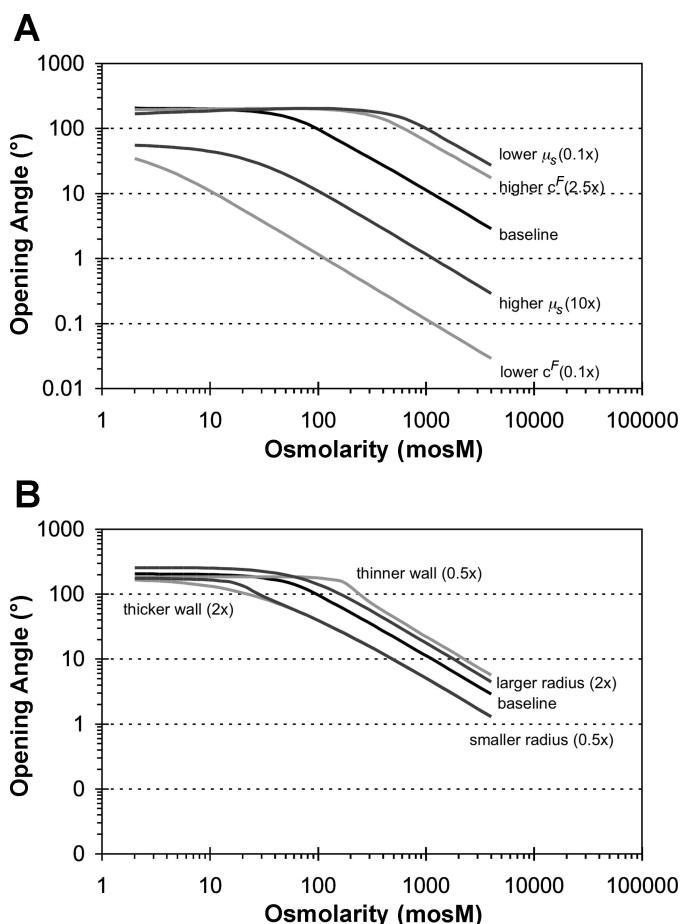
Fig. 2. Opening angle of the cut aortic ring vs. $\bar{c}^*$, from the finite element model, for all 30 increments of $\bar{c}^*$ from 2 to 4,000 mosM; note the log-log scale. Baseline parameters used in the model are as follows: radius of 1.92 mm, wall thickness of 137 μm, maximum fixed-charge density (c^F) of 40 meq/l in the intima and media layers ($c^F = 0$ in the adventitia), and uniform shear modulus (μ_s) of 140 kPa. Effects of altering the maximum fixed-charge density and shear modulus (*A*) and the aortic ring geometry (*B*) by the scaling factors indicated in parentheses are also shown.

−1, implies an inverse relation between the opening angle and the osmolarity.

Variations from the baseline configuration show that, all else being equal, the opening angle increases with increasing fixed-charge density or decreasing shear modulus (Fig. 2*A*). In addition, the opening angle is affected by the geometry of the aortic ring such that it increases with thinner arterial walls or larger arterial diameters (Fig. 2*B*). The opening angle also increases with thinner slices, although only under hypotonic conditions (not shown). Using the isotropic Fung-type exponential strain energy function rather than the neo-Hookean form had a negligible impact on the predicted effect of osmolarity on opening angle, producing no greater than a 9% difference relative to the baseline results presented in Fig. 2.

Experiments. Histological analyses confirmed the heterogeneous distribution of fixed-charge density as determined from Safranin-O staining, with the highest proteoglycan content observed in the media and intima as identified from hematoxylin and eosin staining (Fig. 3). A total of 37 aortic rings were obtained from four animals (*n* = 8, 9, 10, 10 from each rat), which were distributed among different osmotic loading pro-
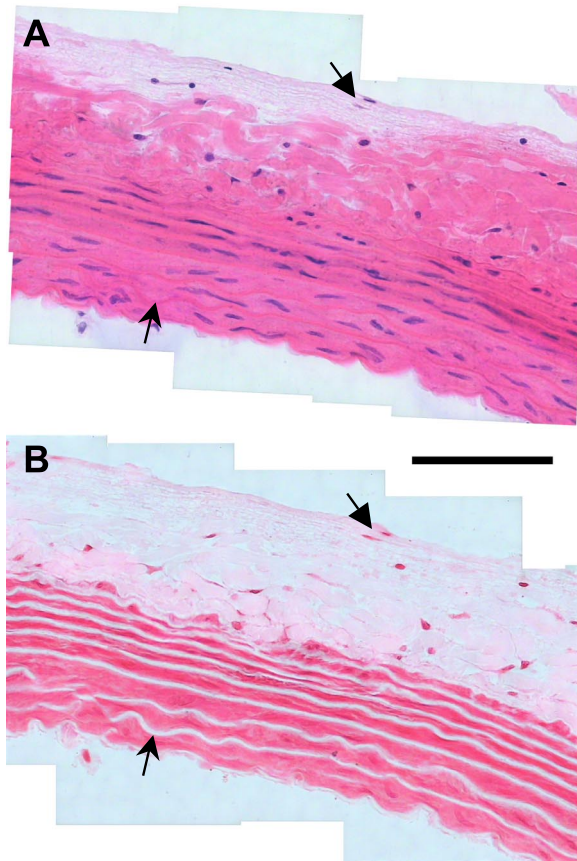

Fig. 1. Geometry of the cut aortic ring at selected external bath osmolarities ($\bar{c}^*$; in mosM), from the finite element analysis. Only one-quarter of the geometry was modeled, due to symmetry.

Fig. 3. Montage of light micrographs (×40 objective) of two 5-μm-thick serial sections of rat aorta. *A*: hematoxylin and eosin staining shows a nonuniform layered extracellular matrix and highly cellularized structure. *B*: Safranin-O staining (intense red) of the adjacent tissue section highlights the heterogeneous radial distribution of glycosaminoglycans, with highest expression of negative fixed charge within the medial layer. The collagenous adventitia, which is clearly visible in *A*, is mostly unstained with Safranin-O. Arrows indicate common structures to help register the 2 sequential tissue sections. Scale bar = 100 μm.

Sample images of a representative aortic ring (Fig. 4*A*) in the unloaded state and after a radial cut and 30-min exposures to hypotonic ($\bar{c}^* = 0$ mosM), isotonic ($\bar{c}^* = 300$ mosM), and hypertonic ($\bar{c}^* = 2,000$ mosM) solutions clearly show substantial decreases in opening angle with increasing solution osmolarity, consistent with the above finite element model results. Average data ($n = 8$ per protocol) throughout the time course of the two converse osmotic challenge protocols described in EXPERIMENTAL MATERIALS AND METHODS (Fig. 4*B*) demonstrate several key features of the experiment. First, the opening angle equilibrates to a new value well within the first 10 min of exposure to each 30-min osmotic challenge. Second, the opening angle returns to a reproducible reference configuration when exposed to isotonic saline at multiple time points during the experimental protocol. Third, symmetry of the two converse protocols revealed that the opening angle is essentially independent of the osmotic loading history. That is, the angle change due to hypotonic loading was not significantly affected by whether it occurred before or after hypertonic loading, and the same was true for the angle change due to hypertonic loading.

To analyze the results of the above experiments, opening angle measurements were averaged from the three 10-min time points in each loading cycle for each aortic ring. Furthermore, because the loading history effects were insignificant ($P > 0.55$), results from the two converse protocols were combined for analysis. The opening angle was $15 \pm 17°$ ($n = 16$) at the 60-min equilibrium point and exhibited similar variability at other bath concentrations (Fig. 5), which is mainly attributed to
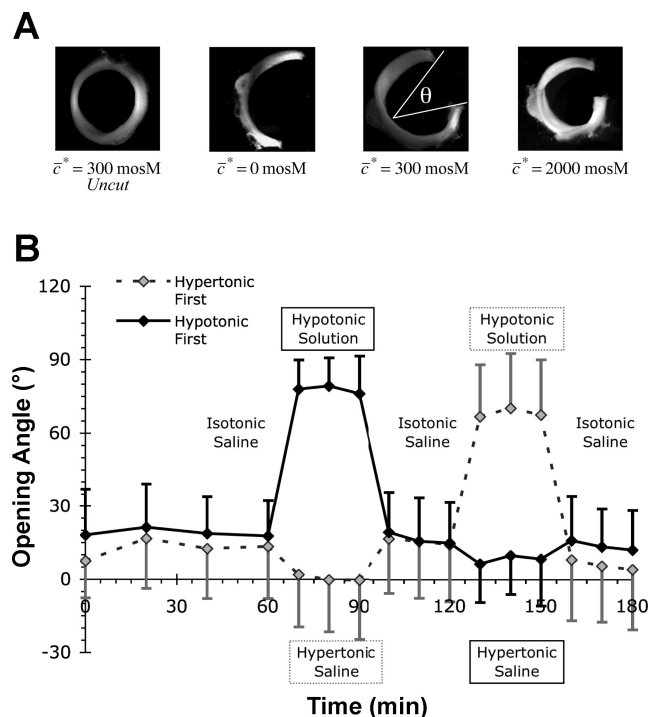

Fig. 4. *A*: representative images of an uncut aortic ring in isotonic 300 mosM solution and the radially cut ring in 0, 300, and 2,000 mosM ionic solutions. The opening angle measurement (θ) is indicated for the 300 mosM cut ring. *B*: time course of opening angle during the 2 converse osmotic loading protocols. Data points represent means ± SD for $n = 8$ samples in each protocol. The cut aortic ring sequence in *A* follows a portion of the protocol indicated by the solid line in *B*.

tocols (8 hypertonic-first saline loading protocol, 8 hypotonic-first saline loading protocol, 11 sucrose loading protocol) or kept as controls (5 with cytochalasin D, 5 without). Consequently, all four rat aortas were comparably represented in each protocol. The tested rings ($n = 37$) had an overall average outer diameter of $1,873 \pm 178$ μm, wall thickness of 120 ± 18 μm, and slice thickness of 996 ± 193 μm in the unloaded state.

Results from the DMMB assay yielded a GAG content of $1.37 \pm 0.23\%$ per dry weight of tissue. The water content was measured at $58 \pm 9\%$, yielding a GAG per wet weight of $0.58 \pm 0.17\%$. With two negative charges and a molecular weight of 513 g/mol per chondroitin sulfate isomer, these results yielded a fixed-charge density of c^F 42 ± 19 meq/l via the formula

$$c^F = \frac{\text{GAG charge number}}{\text{GAG molecular weight}} \times \frac{\text{GAG mass}}{\text{water volume}} \quad (16)$$

This reported value of c^F represents an average across the entire thickness of the aortic wall. From the GAG distribution across the wall (Fig. 3), it can be estimated that c^F is approximately twice this average value in the intima and media and nearly zero in the adventitia.
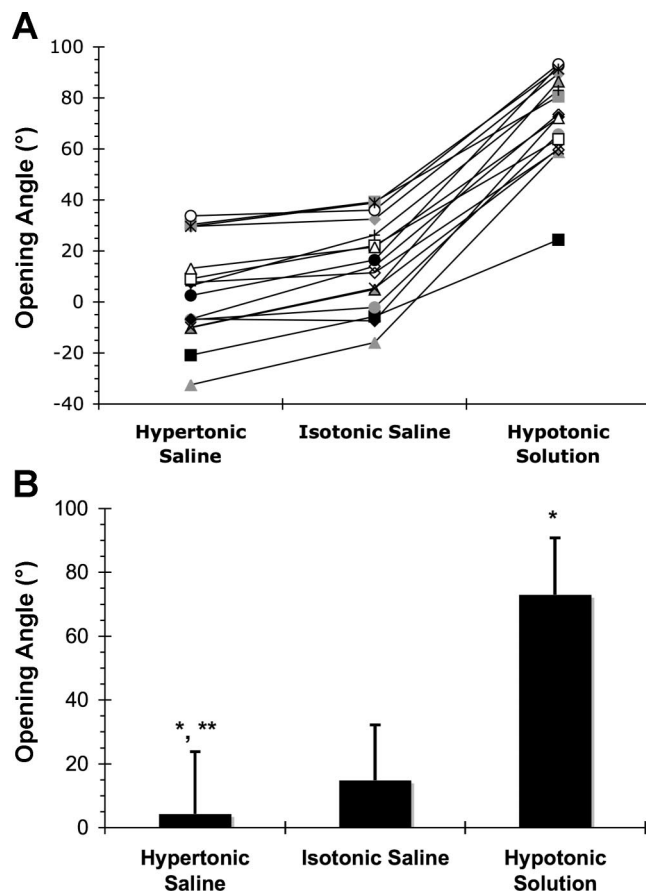
Fig. 5. Saline osmotic challenge. *A*: opening angle data for individual aortic ring samples (*n* = 16) obtained during 30-min exposures to hypertonic saline (2,000 mosM NaCl), isotonic saline (300 mosM NaCl), and hypotonic solution (0 mosM NaCl). *B*: mean opening angle (±SD) corresponding to data in *A*. *$P < 0.002$ vs. isotonic saline; **$P < 0.001$ vs. hypotonic solution.

overall average change in opening angle was $-2.1 \pm 1.5°$ with cytochalasin D and $0.8 \pm 1.6°$ without (data not shown). These changes were not statistically significant compared with zero, and cytochalasin D was found to have no effect on the opening angle over the observed time period.

DISCUSSION

The hypothesis of this study is that the transmural distribution of proteoglycans plays a significant role in regulating the residual stresses in the arterial wall. These residual stresses are hypothesized to arise from the fixed-charge density of the proteoglycans, which induce a Donnan osmotic pressure relative to the external environment. With an inhomogeneous distribution of these proteoglycans through the wall thickness, the Donnan osmotic pressure would also vary through the wall thickness, and the resulting inhomogeneous swelling stress of the solid matrix significantly influences the opening angle observed experimentally.

The first aim of this study was to verify from theory that the hypothesized mechanism could indeed explain the opening angle observed experimentally. Using the triphasic theory of Lai et al. (28) and representative values of the shear modulus of the rat arterial wall (11) and proteoglycan fixed-charge
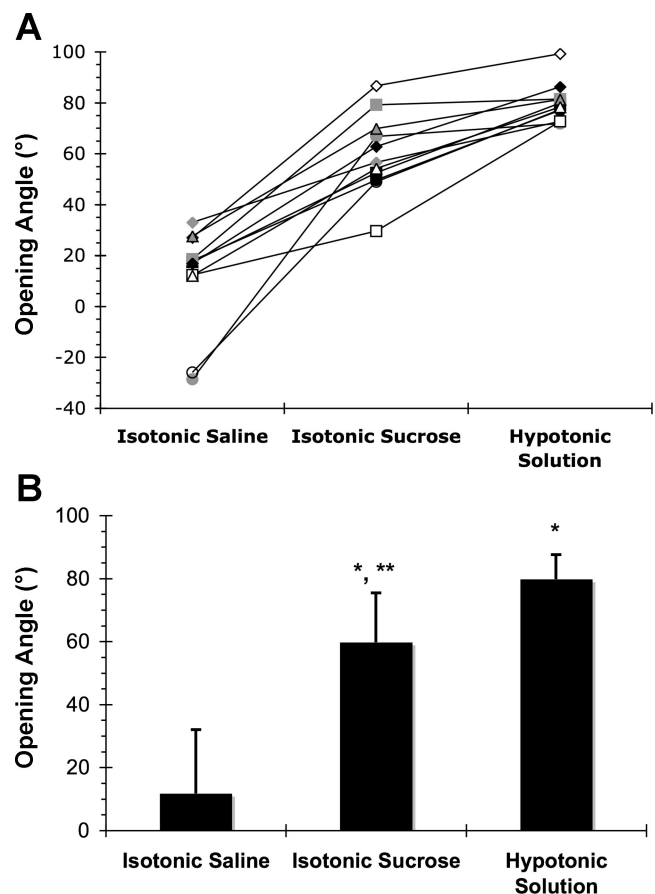
regional heterogeneity with anatomic location along the length of the aorta (31).

As illustrated in Fig. 5, the opening angle during saline osmotic challenge experiments was $73 \pm 18°$ for hypotonic solution (*n* = 16) and $4 \pm 19°$ for hypertonic saline (*n* = 16), both of which were significantly different ($P = 0.001$ and 0.002, respectively) compared with results shown with isotonic saline conditions and each other ($P = 0.001$). In the second group of aortic rings (Fig. 6), when isotonic NaCl solution was replaced with isotonic sucrose, the mean opening angle changed from $12 \pm 20°$ to $60 \pm 16°$ (*n* = 11), which was significant ($P = 0.001$). Opening angle on these same rings became $80 \pm 8°$ under hypotonic conditions, which was a small but significant increase compared with isotonic sucrose ($P = 0.001$). Although the percent variabilities were relatively large, the consistent trends in opening angle during the osmotic challenges were clear when the samples were visualized individually (Fig. 5*A* and Fig. 6*A*).

Two separate control groups that were left in 300 mosM isotonic NaCl, either with or without 4 μM cytochalasin D, had mean opening angles of $13 \pm 24°$ and $10 \pm 25°$ (*n* = 5 per protocol) at the end of the 60-min equilibrium period. These samples, which were kept under isotonic conditions for the entire 180-min duration of the experiment, showed no significant variations in opening angle with time, such that the

Fig. 6. Sucrose challenge. *A*: opening angle data for individual aortic ring samples (*n* = 11) obtained during 30-min exposures to isotonic saline (300 mosM NaCl), isotonic sucrose (300 mosM sucrose), and hypotonic solution (0 mosM NaCl). *B*: corresponding mean opening angle (±SD) increased significantly when rings were moved from isotonic saline to isotonic sucrose (*$P < 0.001$ vs. isotonic saline). There was a small but significant difference between isotonic sucrose and hypotonic solution (**$P < 0.001$).

density (37), it was confirmed that this hypothesized mechanism could readily yield opening angles in the range of experimental values previously reported in the literature (Fig. 1). Indeed, in the finite element simulations, large variations could be obtained in the opening angle under isotonic conditions, by varying the magnitude of the fixed-charge density in the intima and media. Changing the shear modulus or geometry of the ring also influenced the opening angle (Fig. 2).

In particular, the theoretical analysis indicated that varying the ionic strength of the bathing environment could produce large changes in the opening angle (Fig. 2), thereby suggesting a similar experimental design for verifying this hypothesis. In fact, a similar experiment was recently reported in which increasing osmolarity caused a decrease in aortic opening angle (20), although this was attributed to cellular volume changes, which is inconsistent with our findings as discussed below. It is important to recall that the theoretical analysis would not predict changes in the opening angle when the fixed-charge density is uniformly distributed across the wall thickness; in that case, the only effect of changing the ionic strength of the external bath would be to produce uniform swelling or shrinking of the aortic ring, according to *Eq. 15*.

In the second component of this study, histological sections of the rat arterial wall confirmed that the fixed-charge density of the proteoglycans is confined primarily to the intima and media (Fig. 3), consistent with earlier studies (9, 56). These proteoglycans are synthesized by vascular smooth muscle cells and endothelial cells (5, 7, 25); their glycosaminoglycans include the negatively charged chondroitin sulfate, dermatan sulfate, and heparan sulfate (24, 26, 27). The chondroitin sulfate can form large proteoglycans called versican (57), which can aggregate with hyaluronan (13). These biochemical and histological characterizations confirm the presence of an inhomogeneous distribution of fixed-charge density across the arterial wall, which is a necessary condition for the hypothesis of this study to be correct. Biochemical analysis of GAG content in the rat aorta yielded values of the fixed-charge density comparable to those reported by Porterfield et al. (37) in thoracic and abdominal segments of chicken aortas, which were used in our finite element analysis. The GAG content of rat aorta, 0.58% per wet weight, is ~10 times smaller than in human and animal articular cartilage (35).

In the third part of this study, experimental measurements of the opening angle of rat aorta under various bathing solution concentrations of NaCl confirmed the theoretical prediction that the opening angle should increase with decreasing salt concentration (Figs. 1 and 5). From the theoretical analysis, this response can be explained by the concomitant increase in swelling pressure in the intima and media, as predicated by *Eq. 2*, which produces a higher swelling strain on the inner region of the aortic ring and causes it to open up when radially cut. On first consideration, this result alone might seem sufficient to confirm the hypothesis of this study. However, because the media and intima are highly cellularized and because the cell membrane is nearly impermeable to Na^+ and Cl^-, there remains the possibility that the observed response to osmotic loading with various concentrations of NaCl can be the result of volume changes due to water uptake or loss from the cell cytoplasm, as suggested by Guo et al. (20), rather than charge-related Donnan osmotic swelling.

By using neutrally charged sucrose as an alternative osmolyte, which is known to be plasma membrane impermeant (6), it was possible to test the counterhypothesis that the observed change in opening angle resulted from in situ cell swelling, independent of extracellular charge effects. According to this counterhypothesis, osmotic loading of the aortic ring with NaCl and sucrose solutions of equal osmolarities should produce no change in the opening angle, since both should have the same effect on the cell volume. However, when transferring samples from 300 mosM NaCl to 300 mosM sucrose, opening angle was observed to increase very significantly, reaching a mean value within 20° of that obtained with 0 mosM hypotonic solution (Fig. 6). This result implies that most of the change in opening angle (~70%) resulted from charge effects in the extracellular matrix; the small but significant increase from isotonic sucrose to 0 mosM hypotonic solution reflects the contribution of cellular swelling.

From these observations, it is concluded that the inhomogeneous proteoglycan distribution across the aortic wall thickness is a significant contributor to the observed residual stress, thereby confirming the hypothesis of this study. This finding is significant because it provides a clear mechanistic explanation for this residual stress, based on Donnan osmotic swelling theory. It is believed that residual stress in the arterial wall acts to produce a more uniform wall stress distribution when the artery is subjected to physiological internal hydrostatic pressures (8, 22), a condition that is thought to play a role in this tissue's mechanosensory feedback for achieving homeostasis (16). Alterations in luminal blood pressure or flow may disturb this equilibrium condition, and the finding of this study suggests that cells may respond to the resulting altered stress environment by modifying proteoglycan synthesis or degradation, either changing its total content or its distribution across the wall.

This mechanism may be further exacerbated in disease, as suggested by evidence that atherosclerotic plaque has a very high proteoglycan content (14, 40, 51–53). Indeed, the hardening of atherosclerotic arteries can be attributed in part to the increased stiffness imparted by proteoglycans (18), as represented by the osmotic modulus Π in *Eqs. 6 and 9*. These equations also explain the acute decrease in elastic modulus with increasing osmolarity, $\bar{c}^*$, recently reported by Guo et al. (20), and reveal this to be an apparent change due to Donnan osmotic swelling rather than an intrinsic change in the material properties of the tissue solid matrix. Even long-term remodeling of arteries under hypertension was shown to be accompanied by heterogeneous clustering of proteoglycans in the subendothelial and medial layers, resulting in as much as a 164% increase in chondroitin sulfate expression (39). Indeed, it has been observed that the opening angle is higher in aortic rings with visible atheroma (43), consistent with the hypothesis of this study. A recent study looking at multiple single nucleotide polymorphisms in the versican gene found significant associations between such mutations and intracranial aneurysm formation in humans (42). More recently, Heegaard et al. (21) showed that biglycan deficiency in transgenic mice results in aortic dissection and rupture leading to spontaneous death. Our hypothesis coupled with such studies linking cardiovascular disease with charged proteoglycans and vessel biomechanics motivate further investigation of the role of proteoglycans in such pathologies. It should also be noted that our hypothesis is

not limited to cardiovascular biomechanics but may be applicable to any tissues that exhibit inhomogeneous proteoglycan distributions and residual stress.

The results of this study do not imply that residual stresses in the rat aorta can be entirely attributed to nonuniform Donnan osmotic swelling. If this were true, the opening angle should have reduced to zero under hypertonic conditions, whereas individual aortic samples had hypertonic opening angles ranging from $+30°$ to $-30°$ (Fig. 5A). Moreover, preliminary studies using an alternate $LBNF_1$ rat strain (Harlan, Indianapolis, IN) yielded systematically larger opening angles than in Sprague-Dawley rats (hypertonic $66 \pm 22°$, isotonic $88 \pm 26°$, hypotonic $130 \pm 16°$; $n = 15$ slices from 2 $LBNF_1$ rats), although the relative changes in opening angle due to osmotic loading were similar to those shown in the present study. One possibility is that proteoglycans contribute an entropic osmotic pressure, which cannot be entirely alleviated under hypertonic conditions, as observed in measurements of chondroitin sulfate solutions in various osmolarities of NaCl (4, 12). This explanation remains a distinct possibility, although it is expected that entropic effects should be smaller for proteoglycans enmeshed within a solid matrix than in free solution, and this would not explain the observation of negative opening angles in some cases. Therefore, understanding the role of alternative mechanisms that can contribute to residual stress, such as nonuniform growth (41) or heterogeneity of material properties (48), and the underlying reason for the apparent differences in opening angle between rat genetic strains requires further investigation.

It may be argued that an alternative approach for assessing the role of proteoglycans on residual stresses might have used enzymatic degradation to remove them by chemical means. Although this argument is attractive, preliminary studies in our laboratory suggest that treatment with chondroitinase ABC (which degrades chondroitin and dermatan sulfate), hyaluronidase, and heparinase is insufficient to reduce the fixed-charge density to negligible levels, as assessed from histology (data not shown). Furthermore, because residual stresses could only be obtained via heterogeneous distribution of fixed-charge density, a protocol that might lead to homogeneous degradation of proteoglycans, even if significant, might not result in a comparable reduction of opening angle. Although we did not use an exhaustive battery of degradative enzymes or protocols to reach a conclusive outcome on this matter, evidence from articular cartilage biochemistry suggests that nearly complete removal of proteoglycans requires the additional use of trypsin. In the case of the aorta, trypsin would degrade elastin and collagen, potentially confounding the outcome, as other studies have shown that chemical degradation of elastin reduces the opening angle of the aorta (17). Therefore, until a suitable biochemical protocol is found for selectively degrading most proteoglycans in the arterial wall, it may be argued that the osmotic loading protocol adopted in this study provides a more reliable assessment of the role of proteoglycans on residual stress.

In summary, this study proposed and verified the hypothesis that proteoglycans contribute significantly to residual stresses in the arterial wall, by producing an inhomogeneous Donnan osmotic pressure across the wall thickness. This hypothesis was validated from both theory and experiments. A significant implication of this finding is that vascular cells could regulate arterial wall development, growth, and remodeling in response to altered wall stresses via altered deposition or degradation of proteoglycans across the wall thickness, hence modifying the zero-stress state of the tissue. An interesting corollary hypothesis, which remains to be tested, is whether the variation in opening angle along the length of the aorta is significantly correlated with the local amount and distribution of proteoglycans.

REFERENCES

1. **Ateshian GA, Chahine NO, Basalo IM, Hung CT.** The correspondence between equilibrium biphasic and triphasic material properties in mixture models of articular cartilage. *J Biomech* 37: 391–400, 2004.
2. **Ateshian GA, Ellis BJ, Weiss JA.** Equivalence between short-time biphasic and incompressible elastic material responses. *J Biomech Eng* 129: 405, 2007.
3. **Bonet J, Wood RD.** *Nonlinear Continuum Mechanics for Finite Element Analysis.* Cambridge, UK: Cambridge Univ. Press, 1997, p. xvii, 248.
4. **Chahine NO, Chen FH, Hung CT, Ateshian GA.** Direct measurement of osmotic pressure of glycosaminoglycan solutions by membrane osmometry at room temperature. *Biophys J* 89: 1543–1550, 2005.
5. **Chang Y, Yanagishita M, Hascall VC, Wight TN.** Proteoglycans synthesized by smooth muscle cells derived from monkey (*Macaca nemestrina*) aorta. *J Biol Chem* 258: 5679–5688, 1983.
6. **Chao PG, Tang Z, Angelini E, West AC, Costa KD, Hung CT.** Dynamic osmotic loading of chondrocytes using a novel microfluidic device. *J Biomech* 38: 1273–1281, 2005.
7. **Chen K, Wight TN.** Proteoglycans in arterial smooth muscle cell cultures: an ultrastructural histochemical analysis. *J Histochem Cytochem* 32: 347–357, 1984.
8. **Chuong CJ, Fung YC.** On residual stresses in arteries. *J Biomech Eng* 108: 189–192, 1986.
9. **Clowes AW, Clowes MM, Gown AM, Wight TN.** Localization of proteoheparan sulfate in rat aorta. *Histochemistry* 80: 379–384, 1984.
10. **Currier A, He QC, Zysset P.** Conewise linear elastic materials. *J Elasticity* 37: 1–38, 1995.
11. **Deng SX, Tomioka J, Debes JC, Fung YC.** New experiments on shear modulus of elasticity of arteries. *Am J Physiol Heart Circ Physiol* 266: H1–H10, 1994.
12. **Ehrlich S, Wolff N, Schneiderman R, Maroudas A, Parker KH, Winlove CP.** The osmotic pressure of chondroitin sulphate solutions: experimental measurements and theoretical analysis. *Biorheology* 35: 383–397, 1998.
13. **Evanko SP, Johnson PY, Braun KR, Underhill CB, Dudhia J, Wight TN.** Platelet-derived growth factor stimulates the formation of versican-hyaluronan aggregates and pericellular matrix expansion in arterial smooth muscle cells. *Arch Biochem Biophys* 394: 29–38, 2001.
14. **Evanko SP, Raines EW, Ross R, Gold LI, Wight TN.** Proteoglycan distribution in lesions of atherosclerosis depends on lesion severity, structural characteristics, and the proximity of platelet-derived growth factor and transforming growth factor-β. *Am J Pathol* 152: 533–546, 1998.
15. **Farndale RW, Sayers CA, Barrett AJ.** A direct spectrophotometric microassay for sulfated glycosaminoglycans in cartilage cultures. *Connect Tissue Res* 9: 247–248, 1982.
16. **Fung YC.** *Biomechanics: Motion, Flow, Stress, Growth.* New York: Springer-Verlag, 1990, p. xii, 569.

17. **Greenwald SE, Moore JE Jr, Rachev A, Kane TP, Meister JJ.** Experimental investigation of the distribution of residual strains in the artery wall. *J Biomech Eng* 119: 438–444, 1997.

18. **Grodzinsky AJ.** Electromechanical and physicochemical properties of connective tissue. *Crit Rev Biomed Eng* 9: 133–199, 1983.

19. **Guo X, Kassab GS.** Variation of mechanical properties along the length of the aorta in C57bl/6 mice. *Am J Physiol Heart Circ Physiol* 285: H2614–H2622, 2003.

20. **Guo X, Lanir Y, Kassab GS.** Effect of osmolarity on the zero-stress state and mechanical properties of aorta in various species. *Am J Physiol Heart Circ Physiol* 293: H2328–H2334, 2007.

21. **Heegaard AM, Corsi A, Danielsen CC, Nielsen KL, Jorgensen HL, Riminucci M, Young MF, Bianco P.** Biglycan deficiency causes spontaneous aortic dissection and rupture in mice. *Circulation* 115: 2731–2738, 2007.

22. **Humphrey JD.** *Cardiovascular Solid Mechanics: Cells, Tissues, and Organs.* New York: Springer-Verlag, 2002, p. xvi, 757.

23. **Kang T, Yin FC.** The need to account for residual strains and composite nature of heart wall in mechanical analyses. *Am J Physiol Heart Circ Physiol* 271: H947–H961, 1996.

24. **Kapoor R, Phelps CF, Wight TN.** Physical properties of chondroitin sulphate/dermatan sulphate proteoglycans from bovine aorta. *Biochem J* 240: 575–583, 1986.

25. **Kinsella MG, Wight TN.** Formation of high molecular weight dermatan sulfate proteoglycan in bovine aortic endothelial cell cultures. Evidence for transglutaminase-catalyzed cross-linking to fibronectin. *J Biol Chem* 265: 17891–17898, 1990.

26. **Kinsella MG, Wight TN.** Modulation of sulfated proteoglycan synthesis by bovine aortic endothelial cells during migration. *J Cell Biol* 102: 679–687, 1986.

27. **Kinsella MG, Wight TN.** Structural characterization of heparan sulfate proteoglycan subclasses isolated from bovine aortic endothelial cell cultures. *Biochemistry* 27: 2136–2144, 1988.

28. **Lai WM, Hou JS, Mow VC.** A triphasic theory for the swelling and deformation behaviors of articular cartilage. *J Biomech Eng* 113: 245–258, 1991.

29. **Lanir Y, Hayam G, Abovsky M, Zlotnick AY, Uretzky G, Nevo E, Ben-Haim SA.** Effect of myocardial swelling on residual strain in the left ventricle of the rat. *Am J Physiol Heart Circ Physiol* 270: H1736–H1743, 1996.

30. **Liu SQ, Fung YC.** Changes in the structure and mechanical properties of pulmonary arteries of rats exposed to cigarette smoke. *Am Rev Respir Dis* 148: 768–777, 1993.

31. **Liu SQ, Fung YC.** Relationship between hypertension, hypertrophy, and opening angle of zero-stress state of arteries following aortic constriction. *J Biomech Eng* 111: 325–335, 1989.

32. **Lu X, Zhao JB, Wang GR, Gregersen H, Kassab GS.** Remodeling of the zero-stress state of femoral arteries in response to flow overload. *Am J Physiol Heart Circ Physiol* 280: H1547–H1559, 2001.

33. **Maroudas AI.** Balance between swelling pressure and collagen tension in normal and degenerate cartilage. *Nature* 260: 808–809, 1976.

34. **Matsumoto T, Hayashi K.** Stress and strain distribution in hypertensive and normotensive rat aorta considering residual strain. *J Biomech Eng* 118: 62–73, 1996.

35. **Mow VC, Ratcliffe A.** Structure and function of articular cartilage and meniscus. In: *Basic Orthopaedic Biomechanics*, edited by Mow VC, Hayes WC. Philadelphia, PA: Lippincott-Raven, 1997, p. 113–177.

36. **Overbeek JT.** The Donnan equilibrium. *Prog Biophys Biophys Chem* 6: 57–84, 1956.

37. **Porterfield SP, Calhoon TB, Weiss HS.** Changes in connective tissue colloidal charge density with atherosclerosis and age. *J Physiol* 215: 324–329, 1968.

38. **Rachev A, Greenwald SE.** Residual strains in conduit arteries. *J Biomech* 36: 661–670, 2003.

39. **Reynertson RH, Parmley RT, Roden L, Oparil S.** Proteoglycans and hypertension. I. A biochemical and ultrastructural study of aorta glycosaminoglycans in spontaneously hypertensive rats. *Coll Relat Res* 6: 77–101, 1986.

40. **Riessen R, Isner JM, Blessing E, Loushin C, Nikol S, Wight TN.** Regional differences in the distribution of the proteoglycans biglycan and decorin in the extracellular matrix of atherosclerotic and restenotic human coronary arteries. *Am J Pathol* 144: 962–974, 1994.

41. **Rodriguez EK, Hoger A, McCulloch AD.** Stress-dependent finite growth in soft elastic tissues. *J Biomech* 27: 455–467, 1994.

42. **Ruigrok YM, Rinkel GJ, Wijmenga C.** The versican gene and the risk of intracranial aneurysms. *Stroke* 37: 2372–2374, 2006.

43. **Saini A, Berry C, Greenwald S.** Effect of age and sex on residual stress in the aorta. *J Vasc Res* 32: 398–405, 1995.

44. **Seibel MJ, Macaulay W, Jelsma R, Saed-Nejad F, Ratcliffe A.** Antigenic properties of keratan sulfate: influence of antigen structure, monoclonal antibodies, and antibody valency. *Arch Biochem Biophys* 296: 410–418, 1992.

45. **Setton LA, Tohyama H, Mow VC.** Swelling and curling behaviors of articular cartilage. *J Biomech Eng* 120: 355–361, 1998.

46. **Skalak R, Dasgupta G, Moss M, Otten E, Dullumeijer P, Vilmann H.** Analytical description of growth. *J Theor Biol* 94: 555–577, 1982.

47. **Taber LA.** Biomechanics of growth, remodeling, and morphogenesis. *Appl Mech Rev* 48: 487, 1995.

48. **Taber LA, Humphrey JD.** Stress-modulated growth, residual stress, and vascular heterogeneity. *J Biomech Eng* 123: 528–535, 2001.

49. **Takamizawa K, Hayashi K.** Strain energy density function and uniform strain hypothesis for arterial mechanics. *J Biomech* 20: 7–17, 1987.

50. **Tong P, Fung YC.** The stress-strain relationship for the skin. *J Biomech* 9: 649–657, 1976.

51. **Velleman SG, Bacon W, Whitmoyer R, Hosso SJ.** Changes in distribution of glycosaminoglycans during the progression of cholesterol induced atherosclerosis in Japanese quail. *Atherosclerosis* 137: 63–70, 1998.

52. **Vijayagopal P, Figueroa JE, Fontenot JD, Glancy DL.** Isolation and characterization of a proteoglycan variant from human aorta exhibiting a marked affinity for low density lipoprotein and demonstration of its enhanced expression in atherosclerotic plaques. *Atherosclerosis* 127: 195–203, 1996.

53. **Volker W, Schmidt A, Oortmann W, Broszey T, Faber V, Buddecke E.** Mapping of proteoglycans in atherosclerotic lesions. *Eur Heart J* 11, *Suppl* E: 29–40, 1990.

54. **Wagenseil JE, Nerurkar NL, Knutsen RH, Okamoto RJ, Li DY, Mecham RP.** Effects of elastin haploinsufficiency on the mechanical behavior of mouse arteries. *Am J Physiol Heart Circ Physiol* 289: H1209–H1217, 2005.

55. **Weiss TF.** *Cellular Biophysics.* Cambridge, MA: MIT, 1996, p. v.

56. **Wight TN.** Vessel proteoglycans and thrombogenesis. *Prog Hemost Thromb* 5: 1–39, 1980.

57. **Yao LY, Moody C, Schonherr E, Wight TN, Sandell LJ.** Identification of the proteoglycan versican in aorta and smooth muscle cells by DNA sequence analysis, in situ hybridization and immunohistochemistry. *Matrix Biol* 14: 213–225, 1994.